Int J Legal Med (2017) 131:1675–1690
DOI 10.1007/s00414-017-1555-0

REVIEW

Elliptical Fourier analysis: fundamentals, applications, and value for forensic anthropology

Jodi Caple[1] · **John Byrd**[2] · **Carl N. Stephan**[1]

Received: 12 December 2016 / Accepted: 2 February 2017 / Published online: 17 February 2017

Abstract The numerical description of skeletal morphology enables forensic anthropologists to conduct objective, reproducible, and structured tests, with the added capability of verifying morphoscopic-based analyses. One technique that permits comprehensive quantification of outline shape is elliptical Fourier analysis. This curve fitting technique allows a form's outline to be approximated via the sum of multiple sine and cosine waves, permitting the profile perimeter of an object to be described in a dense (continuous) manner at a user-defined level of precision. A large amount of shape information (the entire perimeter) can thereby be collected in contrast to other methods relying on sparsely located landmarks where information falling in between the landmarks fails to be acquired. First published in 1982, elliptical Fourier analysis employment in forensic anthropology from 2000 onwards reflects a slow uptake despite large computing power that makes its calculations easy to conduct. Without hurdles arising from calculation speed or quantity, the slow uptake may partly reside with the underlying mathematics that on first glance is extensive and potentially intimidating. In this paper, we aim to bridge this gap by pictorially illustrating how elliptical Fourier harmonics work in a simple step-by-step visual fashion to facilitate universal understanding and as geared towards increased use in forensic anthropology. We additionally provide a short review of the method's utility for osteology, a summary of past uses in forensic anthropology, and software options for calculations that largely save the user the trouble of coding customized routines.

Keywords Forensic science · Outline analysis · Quantification · Form · Size · Shape

Introduction

Elliptical Fourier analysis (EFA) is a mathematical tool developed in 1982 by Kuhl and Giardina [1] to quantitatively describe a closed outline, such as that of a morphological form, at a user-specified level of detail. This is achieved using two sets of partial differential equations comprised of sine and cosine terms. The EFA method of Kuhl and Giardina represents an extension of the regular Fourier series, first derived by Jean Baptiste Joseph Fourier (1768–1830) that elegantly describes periodic or oscillating functions, i.e., repeating patterns along a time axis. For example, by tracing a static 2D outline shape and recording just the *x*-axis position value by time, a repeating pattern or periodic function is generated as the outline is retraced multiple times. Fourier's breakthrough was so revolutionary and general in its application that at the time it was discovered, it was not accepted by leading physicists (e.g., Biot, Laplace, and Poisson)—because it was thought to be too impressive to be believed, delaying its publication by approximately 15 years [2]. While Fourier's original interest was heat transfer, it was Cosgriff [3] who first recognized that closed contours could too be treated as periodic (repeating) patterns, permitting the transformation of spatial geometrical

Electronic supplementary material The online version of this article (doi:10.1007/s00414-017-1555-0) contains supplementary material, which is available to authorized users.

✉ Jodi Caple
jodi.caple@uqconnect.edu.au

[1] Laboratory for Human Craniofacial and Skeletal Identification (HuCS-ID Lab), School of Biomedical Sciences, The University of Queensland, Brisbane, QLD 4072, Australia

[2] Defense Prisoner of War/Missing in Action Accounting Agency, 590 Moffet St., Building 4077, Joint Base Pearl Harbor-Hickam, Oahu, HI 96853, USA

data into the frequency domain. This subsequently paved the way for Kuhl and Giardina's formulation of EFA.

One of the first practical applications of Kuhl and Giardina's shape description method was in the detection of airplane silhouettes from radar images [1]. Since its development in 1982, EFA has experienced a slow uptake in forensic anthropology with its first published use in 2000 [4]. Where classification accuracies exist for multiple methods for assigning biological characters (e.g., sex and/or ancestry using morphoscopic trait or linear measurement analysis), EFA often performs comparably or better (see Table 1), signaling broad but currently unrealized utility. The limited use may be a result of the mathematical complexity by which EFA is typically described. Indeed, many explanations of EFA (e.g., [1, 5–10]) assume more than a basic or elementary level of mathematics, especially as pertains to the level of the general biologist, impeding understanding where technical jargon is employed—"piecewise constant derivatives" [1] are but one example from the literature. While some good basic descriptions of regular Fourier series exist for the non-mathematician (e.g., [11]), there appears to be no equivalent for elliptical Fourier analysis. So too, the similarities and differences of regular Fourier series and elliptical Fourier analysis tend not to be clearly illustrated for non-mathematicians. The aim of this paper is to fill this void. Herein, we review EFA in lay terms and provide pictorial explanations to illustrate the most perplexing parts of the mathematical formulae. Additionally, we provide specific examples of the utility of EFA in forensic anthropology and describe software capabilities.

A short description of the value of the quantification of anatomical morphology

While physical anthropologists are typically very adept at visually, or morphoscopically, assessing human skeletons for biological characteristics (sex, age, and ancestry) and injury (timing, blunt force, and sharp force), the numerical description of morphology is also crucial. Quantified analyses enable objective and structured tests that lend themselves to repeatability and reproducibility, as embodied by the classic example of bone length regression equations for stature estimation [32]. Additionally, quantification serves to offer measurable data that may verify principles of morphoscopic analyses, and the numerical product from quantitative analysis enables computer-automated analysis of large datasets, which can be extremely useful. While in some cases morphoscopic analyses may be the ultimate preference due to their low cost, ease (for trained individuals), speed, and (in some cases) accuracy, it is prudent wherever possible for the underlying principles on which the morphoscopic analysis rests to be verified quantitatively. The repeatability and reproducibility measurements derived from quantification further play an important role for courtroom-based evidentiary standards, as exemplified by the objectives of the Organization of Scientific Area Committees (OSAC) under the US National Institute of Standards and Testing (NIST) and as inspired by the National Academy of Sciences Report on the Forensic Sciences [33].

Before moving onto the mechanics of quantification, it is also important to mention here that "form" is currently used in the literature to encompass all physical attributes of a morphology including, but not limited to, size (scale), shape (outline), and spatial orientation [34] (see Fig. 1). The same usage is found herein.

Approaches to morphological quantification

Initial attempts to quantify skeletal size and shape involved conventional metric approaches using linear distances, angles, and ratios [35]. These simple measurements alone can provide

Table 1 Accuracy of classification for select skeletal features using morphometric and visual methods

Skeletal element	Estimation category	Accuracy (%)		
		Elliptical Fourier analysis	Linear measurements	Visual assessment
Frontal sinus	Individuation	96 [12]	*~100* [13]	100 [14][a]
Anterior nasal aperture	Ancestry	*91–96* [15]	94–95 [15]	83–86 [16][b]
Mandible	Sex	*92–97* [17]	78–81 [18]; 82 [19]; 85 [20]	58–86 [21]
Clavicle	Short-list to assist individuation	75 [22]	–	*88–100* [23][c]
Prox. humerus	Sex	*92–95* [4]	89–90 [24]	83–86 [18]
Greater sciatic notch	Sex	*92* [25]	70–87 [26]; 72–77 [27]	80 [28]; 86 [29]; 88 [30]
Patella	Individuation	91 [31]	–	*97* [31]

Italics indicates the highest method performer for each skeletal feature derived from any kind of validation testing

[a] Reported as 100% accuracy without validation testing

[b] Based on a combination of six mid-facial traits and one cranial trait

[c] Combination of features from the cervicothoracic junction (clavicle and C3–T4 vertebrae)

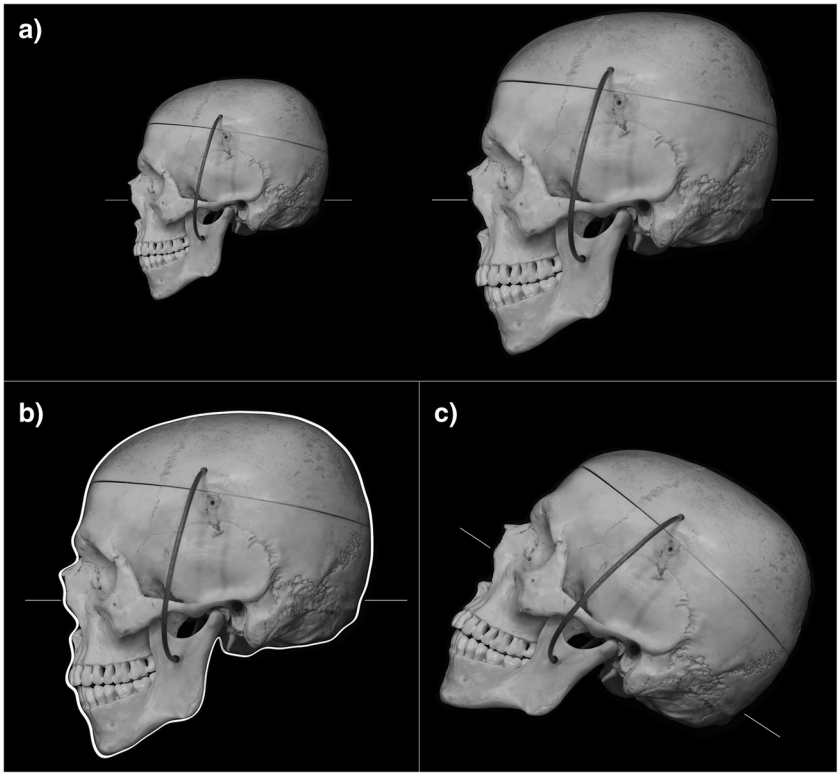

Fig. 1 Components of morphological form. **a** Size. **b** Shape—only perimeter outline highlighted (*white line*). **c** Spatial orientation

for powerful analysis of shape, especially when undertaken in multivariate fashion. Measurements such as these form the underlying basis for classification of unknown skeletal materials in the well-known program FORDISC [36]. While classification accuracies of these methods can be high (depending on the trait(s) evaluated), landmark placement is important in determining the shape information to be retained and fine details of boundary shape information will not be retained if the boundary sampling is sparse—as it often is when linear measurements are employed. This has prompted pursuit of other more comprehensive approaches to shape measurement.

One such method is geometric morphometrics (GMM), which has been traditionally classed as a landmark approach because it requires the placement of a finite set of multiple landmarks at strategic locations that are then subject to analysis. Landmark-based GMM methods include superimposition methods that standardize for rotation, translation, and scale, such as generalized Procrustes [37] and resistant-fit methods [38]; thin plate spline, which mathematically expresses global shape changes on a deformation grid [39]; and Euclidean distance matrix analysis (EDMA), which is a coordinate-free alternative, thus avoiding the coordinate covariation introduced by superimposition [40]. More recently, landmark-based methods have been supplemented by pseudo-landmark and semi-landmark modifications in an attempt to boost point sampling between "real" landmarks and thus the amount of shape information recorded along boundary edges [39, 41].

Rather than placing limited numbers of landmarks at strategic positions, outline methods are also available to more fully describe continuous margins. Depending on the approach, these can be applicable to open or closed outlines. The methods include polynomial curve fitting, Fourier analysis, EFA, and wavelet-based supplementations of the latter approach [42]. Note that contour methods such as EFA are not entirely dissociated from landmark-based methods since they begin with a single landmark to initiate the shape approximation or may use a suite of landmarks distributed around the object boundary to record its shape, and so, differentiation between landmark and non-landmark-based methods cannot be considered to be strictly categorical [43]. After reviewing the mechanics of Fourier and EFA, we will return to consider strengths and weaknesses of this latter method.

Fourier analysis

As mentioned above, Fourier analysis was originally developed to describe radiant heat transfer from solid objects [2]. As a result of this work, Fourier demonstrated that it is possible to reconstruct any complex curve or function by transforming it into the frequency domain and reducing the complex form to a series of more simple sine and cosine components (i.e., simpler waves).

A special example of how a Fourier series can describe a shape by transforming the geometric data from a spatial to a frequency domain is the description of a point traveling

around the outline of a unit circle (radius of one) at constant speed (Fig. 2a). The x and y coordinates can be plotted as a time series (termed a t-axis) [6], with the y-coordinates generating a sine wave (Fig. 2b) and the x-coordinates a cosine wave (Fig. 2c). These simple waves can be combined (summed) to form a single more complex wave that encodes both sets of data (Fig. 2d), and this complex wave can always be decomposed back into its original starting constituents.

Complex waves are neatly described by partial differential equations comprised of two terms that correspond to the sine and cosine waves. This is straightforward for the unit circle, which is precisely described by only one sine and one cosine term; however, additional orders of sine and cosine terms—denoted harmonics—are required for describing more complex patterns/waves as represented by

$$y = f(t) = A_0 + \sum_{n=1}^{k} A_n \cos(nt) + \sum_{n=1}^{k} B_n \sin(nt) \quad (1)$$

where y is the wave amplitude (dependent variable), A_0 is the constant, A_n and B_n are the harmonic coefficients of the nth order, and t represents the points sampled from the t-axis given by the period 2π. The constant and coefficients are derived using further trigonometric functions, not presented here in the interest to maintain simplicity; however, readers can find further details, e.g., in Lestrel [6]. An object's outline shape can be described by an infinite number of harmonics, although the amount of the shape information captured tends to decrease with increasing harmonic order. As the summed or cumulative number of harmonics increases, so does the level of shape detail captured by the Fourier terms (Fig. 3).

In conventional Fourier outline analysis, boundary data are first converted to a new 1D "shape signature" variable, which produces a single time series graph when projected to the frequency domain by its recalculation about the object in time. The most popular shape signature method converts the Cartesian coordinates into radial coordinates using a polar coordinate axis. As this method uses a constant polar angle, with equally dispersed radial lines projecting from the pole (center) to intersect with the object outline (for further information, see [7, 45]), its application is limited to simpler shapes so that multiple intersection points are not generated by instances where the outline curves back upon itself [6]. For descriptions of

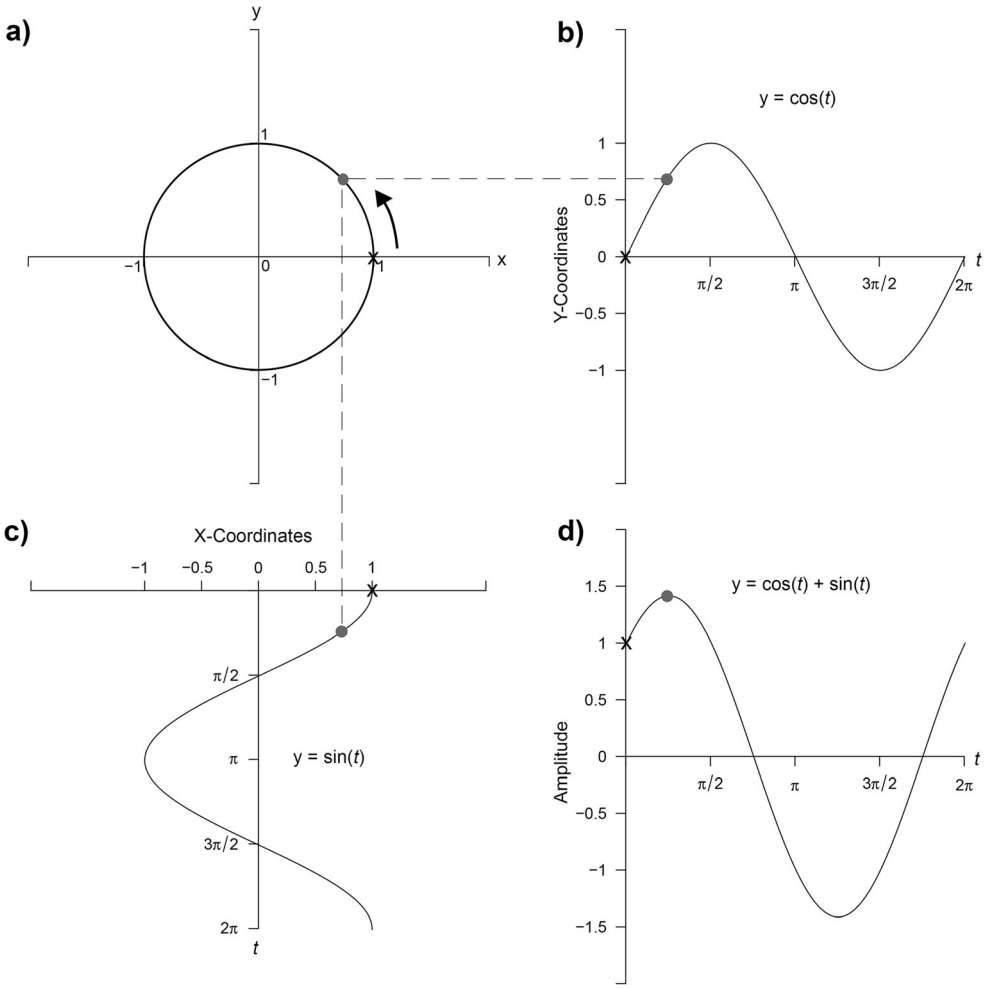

Fig. 2 A unit circle example of frequency encoding of spatial data using the Fourier series. **a** Unit circle plotted on a Cartesian grid with x and y coordinates (*arrow* indicates direction of travel for subsequent graphs). **b**, **c** The projection of the y (**b**) and x coordinates (**c**) of the circle starting at the 1, 0 (x, y) and working counterclockwise (*gray dot* indicates one point in the time series). **d** The summation of **b** and **c** waves into a single complex wave. Example modeled after Transnational College of Lex [11]. Images created using R [44]

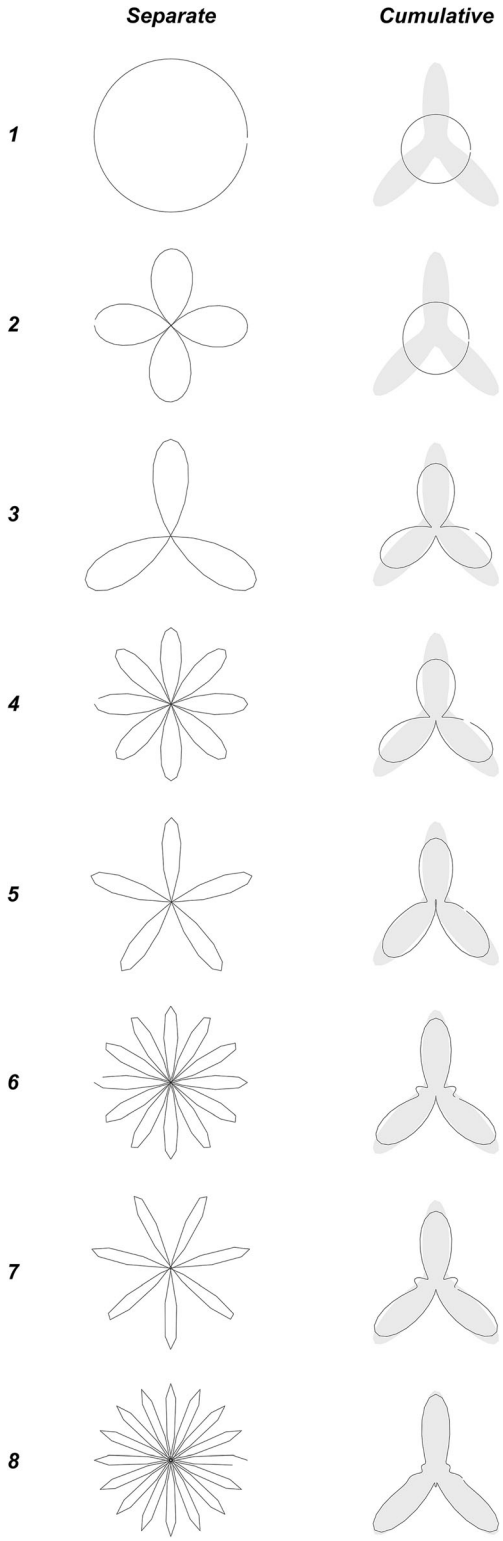

Fig. 3 Harmonic visualization for traditional Fourier outline analysis using polar coordinate data. The first eight harmonics individually plotted for the shape depicted in gray on the right (*Separate*). Relative size information is not retained to aid visualization. Approximation of the original shape outline as subsequent harmonics are combined, showing that the approximation is converging on the original shape (depicted in *gray*) as the harmonic number increases (*Cumulative*). Example modeled after Rohlf and Archie [45]. Images created using R [44]

other shape signature methods, see Rohlf and Archie [45], Zahn and Roskies [46], and Zhang and Lu [47].

Elliptical Fourier analysis

Rather than encoding shape in a single 1D signature and projecting it to the frequency domain as regular Fourier series does (Figs. 2 and 4), EFA uses two signature codes (one for the *x*-coordinates and another for the *y*-coordinates), ingeniously combining the two sets of data to form a chain of interlinked ellipses that move in time about one another. This enables an approximation of the target shape by a single point on the highest order ellipse. This is the key difference that distinguishes regular Fourier series and EFA, as the latter uses two sets of partial differential equations for each harmonic each with sine and cosine terms (i.e., four coefficients in total per harmonic: a_n, b_n, c_n, d_n) so that it can define the harmonic as an ellipse. In contrast, regular Fourier series uses a single shape signature function, such that each harmonic is comprised of only two coefficients (a_n, b_n). Note here that the Fourier coefficients are often termed "Fourier descriptors." For a comparison of traditional and elliptical Fourier analysis methods using the same starting shape, see Fig. 4 and Supplementary Video 1.

To be a little more precise regarding the interactions of the ellipses during EFA, the contour of a shape is described by epicycles—the movement of the center point of any given ellipse (corresponding to harmonic n) around the perimeter of a larger ellipse (harmonic $n - 1$). That is, any given ellipse moves around the perimeter of the ellipse preceding it, which, in turn, moves around the ellipse that precedes that ellipse, and so on until the ellipse for the first harmonic is reached. The end product of the sum of these mechanics is elegant and best illustrated by animation as provided in Supplementary Videos 1–3.

With this overarching concept map of how EFA works, it is worth delving back into some of the finer details of the transition of spatial shape data to the frequency domain in EFA and how this links to regular Fourier series. While it is not our intention here to become too immersed in the details of the trigonometry, for completeness, the mathematics must be at least superficially presented. If non-mathematicians prefer only the pictorial illustrations, then the reader should skip the following paragraph on the partial differential equations.

For EFA, the parametric functions $x(t)$ and $y(t)$ are expanded as follows:

$$x(t) = A_0 + \sum_{n=1}^{k} \left(a_n \cos nt_n + b_n \sin nt_{n-1}\right) \quad (2)$$

and

$$y(t) = C_0 + \sum_{n=1}^{k} \left(c_n \cos nt_n + d_n \sin nt_{n-1}\right) \quad (3)$$

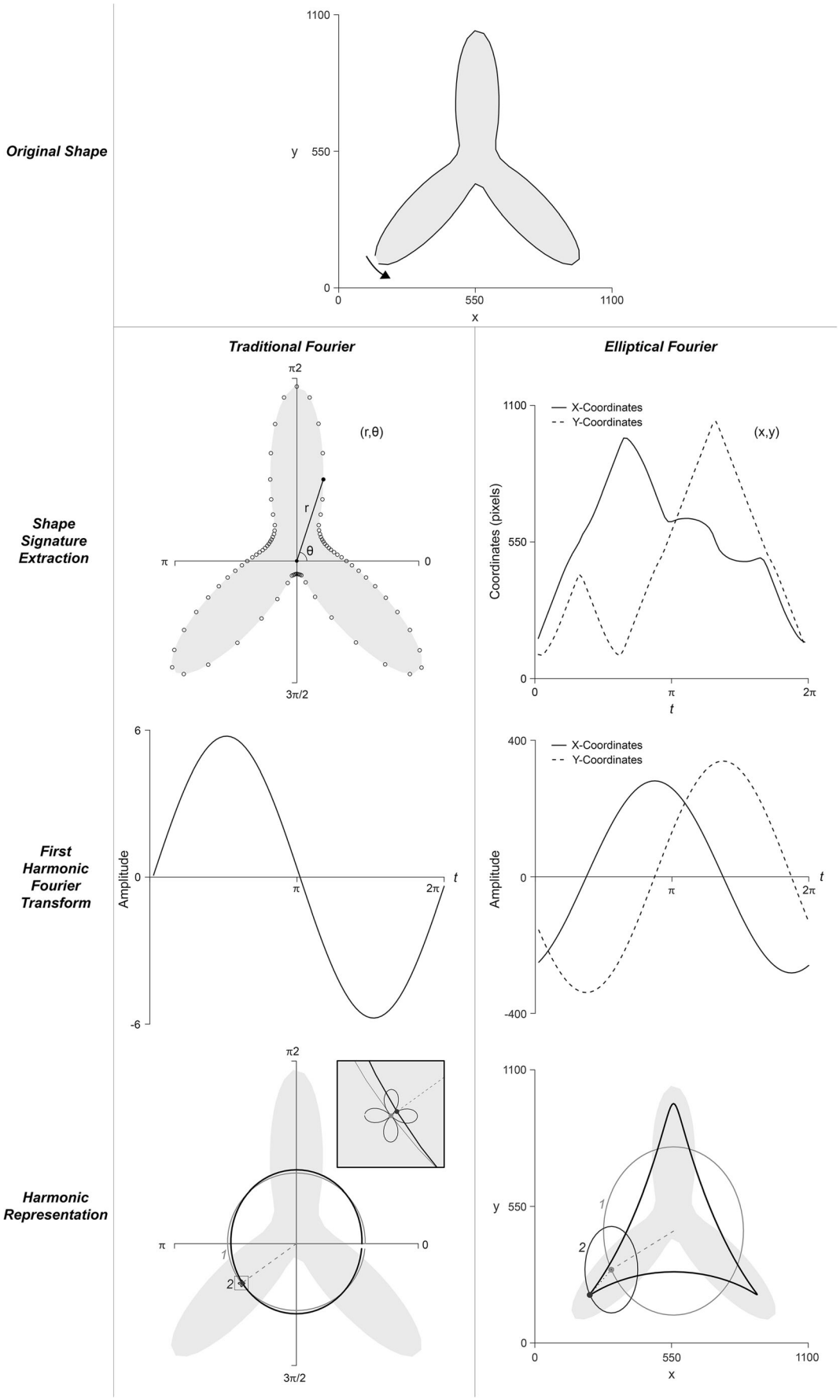
Original Shape
1100
y 550
0
0
550
1100
x
Traditional Fourier
Elliptical Fourier
Shape Signature Extraction
π2
(r,θ)
r
θ
π
0
3π/2
1100
X-Coordinates
Y-Coordinates
(x,y)
Coordinates (pixels)
550
0
0
π
2π
t
First Harmonic Fourier Transform
6
Amplitude
0
-6
π
2π
t
400
X-Coordinates
Y-Coordinates
Amplitude
0
-400
π
2π
t
Harmonic Representation
π2
π
0
1
2
3π/2
1100
y 550
0
1
2
0
550
1100
x

◀**Fig. 4** Comparison of traditional Fourier and elliptical Fourier analysis methods. Original object shape and outline depicted using 80 equally spaced landmarks (*Original Shape*). Methods for extraction of outline information, demonstrating the major difference between traditional and elliptical Fourier methods (*Shape Signature Extraction*). For traditional Fourier, the information is combined into a single function, whereas the *x* and *y* coordinates are analyzed in separate functions for elliptical Fourier. The traditional Fourier shape signature extraction method chosen for this example uses polar coordinates (r = radius, θ = theta angle) between equally spaced angled radii. The elliptical Fourier method plots the *x* and *y* coordinates separately against a new time (t) axis. Complex wave (a combination of sine and cosine terms) for the first harmonic (*First Harmonic Fourier Transform*). Traditional Fourier has one complex wave resulting from a single Fourier function, compared with two for elliptical Fourier (one for each of the *x* and *y* coordinate functions). Reconstructed outline shape approximation depicting the first two harmonics in relation to each other (*Harmonic Representation*). Traditional Fourier is in polar coordinate space, whereas elliptical Fourier is in Cartesian coordinate space. Harmonics are *gray*; phasors are *dotted lines*, and the combined outlines are *bold black lines*. Images created using R [44]

where t is the collective chord length of the outline points, scaled to range from 0 to 2π, (a_n, b_n) and (c_n, d_n) are the four Fourier coefficients defining each harmonic (nth order), and k is the maximum number of harmonics used [6]. A_0 and C_0 are constants that represent the weighted *x* and *y* coordinates of the center of the form, and their equations can be found in Kuhl and Giardina's landmark paper [1] and the appendix to Lestrel's EFA paper [6].

By setting the period $T = 2\pi$, the nth harmonic's coefficients, which are used for subsequent analysis, are represented for the *x*-projection as

$$a_n = 1/n^2\pi \sum_{p=1}^{q} \Delta x_p/\Delta t_p . \left[\cos\left(nt_p\right) - \cos\left(nt_{p-1}\right)\right] \quad (4)$$

and

$$b_n = 1/n^2\pi \sum_{p=1}^{q} \Delta x_p/\Delta t_p . \left[\sin\left(nt_p\right) - \sin\left(nt_{p-1}\right)\right] \quad (5)$$

where the number of outline points (p) total to equal q; t_p is the length of the step between the points p and $p + 1$, and Δx_p is the projection of p to $p + 1$. The *y*-projection Fourier coefficients, c_n and d_n, can be calculated in the same manner as Eqs. (4) and (5), substituting Δx_p for Δy_p.

For any quantitative analysis using EFA, it is the four coefficients (a_n, b_n, c_n, d_n) that are retained as the outline shape descriptors, and they can be used either to reconstruct the starting shape as an approximation or as the basis for statistical assessment of shape—see Table 2 for the EFA coefficients for the first 20 harmonics describing the skull outline shape in Figs. 5, 6, and 7. It should be noted that the mathematics of EFA has been widely trialed and tested over the years and is well recognized to be robust.

Table 2 The Fourier descriptors (coefficients) for the first 20 harmonics calculated using Eqs. (4)–(5) and the skull outline used in Figs. 5, 6, and 7[a]

Harmonic number	a_n	b_n	c_n	d_n
1	−330.422	99.73088	−192.586	−296.596
2	52.83648	6.819893	−61.1977	15.19532
3	−14.916	−1.63322	0.605295	−41.5449
4	−8.28668	−25.3474	26.12699	−8.27207
5	5.008195	−8.50411	8.087178	6.895032
6	2.169348	−0.84613	−1.9586	−1.87794
7	0.148094	6.140658	2.77881	−4.87293
8	−2.78538	−0.11023	5.7206	1.715498
9	0.597155	−0.41022	0.319893	5.283465
10	0.489914	−1.44532	−3.7345	2.231514
11	−0.37304	−0.33243	−2.13588	−0.80122
12	−2.57681	−0.33451	0.480483	−1.16328
13	−3.91576	−1.12792	0.170185	1.534124
14	−3.1378	−0.95338	−1.77637	−0.77887
15	−2.4876	−0.59796	0.949671	−1.76404
16	−1.20013	0.367144	1.926024	0.284832
17	−0.44792	1.146361	−0.59133	0.844731
18	−0.24043	0.628154	−0.44107	−1.2967
19	1.205436	0.55456	1.114009	−1.37115
20	0.943532	0.583383	1.167985	0.527544

[a] Following the equations provided by Lestrel [6], the constants for this inputted shape are as follows:

A_0 = 954.9844; C_0 = 1316.721. Consequently, to calculate the *x* and *y* projections of the original shape (as displayed in Fig. 6c, d), the following would be undertaken for the first harmonic by substitution into Eqs. (2) and (3): $x(t) = 954.9844 + -330.422(\cos{*}1{*}t_n) + 99.73088(\sin{*}1{*}t_{n-1})$; $y(t) = 1316.721 + -192.586(\cos{*}1{*}t_n) + -296.596(\sin{*}1{*}t_{n-1})$. When these data are plotted against each other, they form the large ellipse of the first harmonic observed in Fig. 6e

As previously mentioned, EFA records a form's shape by retaining the *x* and the *y* coordinates separately [6] (Fig. 5) and projecting these data to the frequency domain as waves (Fig. 6a, b). These waves can be represented in their complex form (summed sine and cosine terms; Fig. 6c, d) that when plotted against one another for a corresponding harmonic value generate an ellipse (Fig. 6e). As a result of this process, the first harmonic tends to describe the general size and length of the object being analyzed.

The position of each subsequent harmonic ($n + 1$) is centered on the current time point, but on the previous harmonic (n) (see, e.g., Fig. 7a). These center points travel around the ellipse of the previously set harmonic, establishing a vector from the center of the previous harmonic that is termed a "phasor" by mathematicians. The harmonic number (n) represents the wavelength and, in turn, the number of times the point traverses around that harmonic in the total time period (e.g., this point travels around the second harmonic twice in

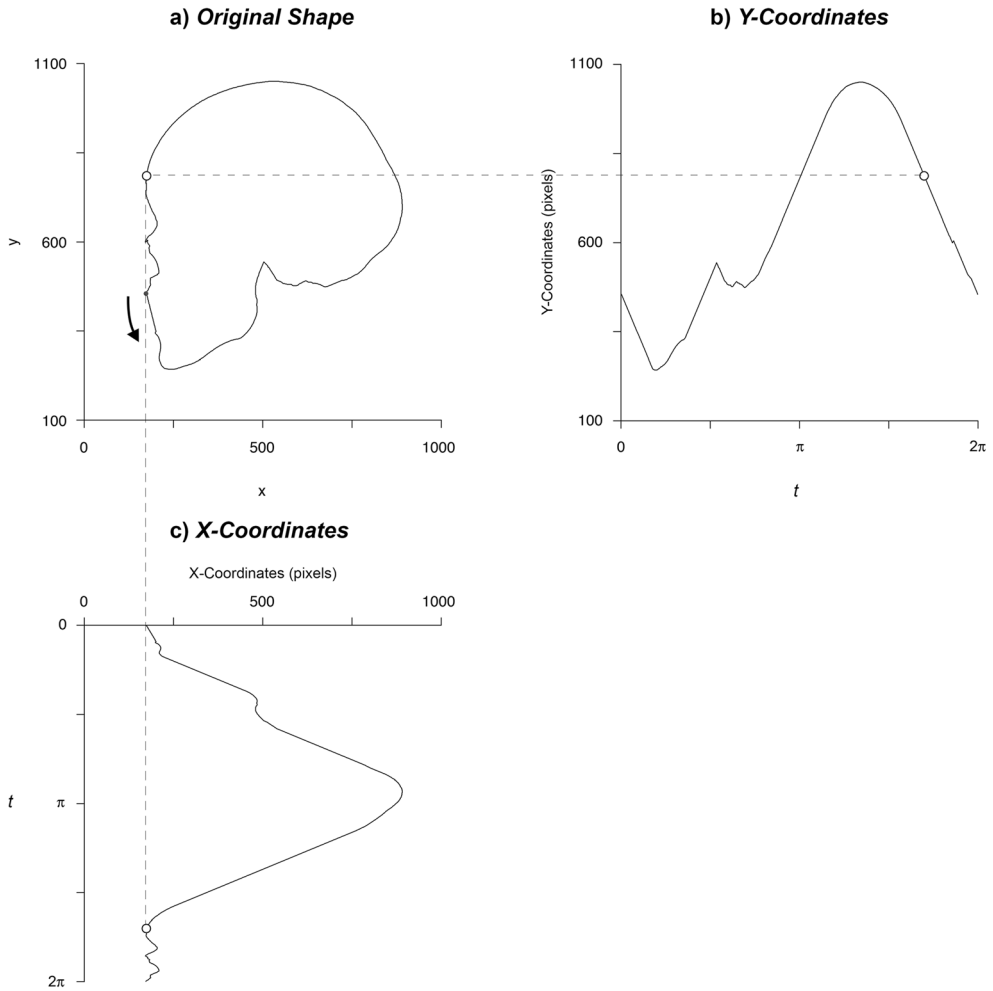

Fig. 5 Starting data for EFA. **a** A left lateral skull outline with *x* and *y* coordinates plotted on a Cartesian axis (spatial domain); *arrow* indicates counterclockwise direction of travel (*Original Shape*). **b** The projection of the *y* coordinates of the skull to a new *t*-axis; the series starts at the *filled circle* and *arrow* in **a** (*Y-Coordinates*). **c** The projection of the *x* coordinates of the skull to a new *t*-axis. The *unfilled circle* depicts an equivalent point in the series (850 out of 1000). Images created using R [44]

the time it takes to traverse the first harmonic). In a similar fashion to traditional Fourier, each additional rotation captures a greater amount of shape detail, thereby improving the shape approximation with increasing harmonic numbers (see Supplementary Videos 1–3). Note that the Fourier coefficients are not dependent on their counterparts in higher or lower harmonics and do not change as the harmonic number is increased. That is, the first two harmonics will remain the same for a shape described by two, three, four, or more harmonics.

The product of any EFA is a matrix of coefficients four cells wide (corresponding to the four coefficients for each harmonic) and as many rows long as harmonics used in the analysis (Table 2). Since ellipses are used, the shape description in EFA is (i) global and (ii) good at replicating natural shapes with curved edges—EFA does not do so well on straight edges and/or acute corners (Fig. 8). As skeletons are natural forms, EFA is well suited to their description. One of the useful properties of these Fourier coefficients resulting from EFA is their inverse transformation, which enables the frequency data to be converted back to the spatial domain providing a visual reconstruction of the EFA geometrical shape approximation (see Figs. 7, 8, and 9). This is useful since it is challenging for humans to interpret tables of Fourier descriptors alone —instead, their visualization tends to be much easier. Such inverse transformations are routinely employed by the majority of EFA studies (see, e.g., [1, 17, 48]). Figure 7 depicts how the harmonics combine to approximate a skull's shape and increase in accuracy with an increased harmonic number.

EFA add-ons

One question that arises when using EFA is how the appropriate number of harmonics is selected for analysis since it determines the EFA approximation accuracy. One way this can be done is to subject the harmonics to the Nyquist frequency sampling rate, which states that the harmonic number must be less than half the number of sampled outline points (variables) [6]. Other methods involve either calculating the percentage of deviation between the reconstructed Fourier outline and the original outline using different harmonic numbers or calculating the cumulative power of the harmonics as shape measures (see [49]).

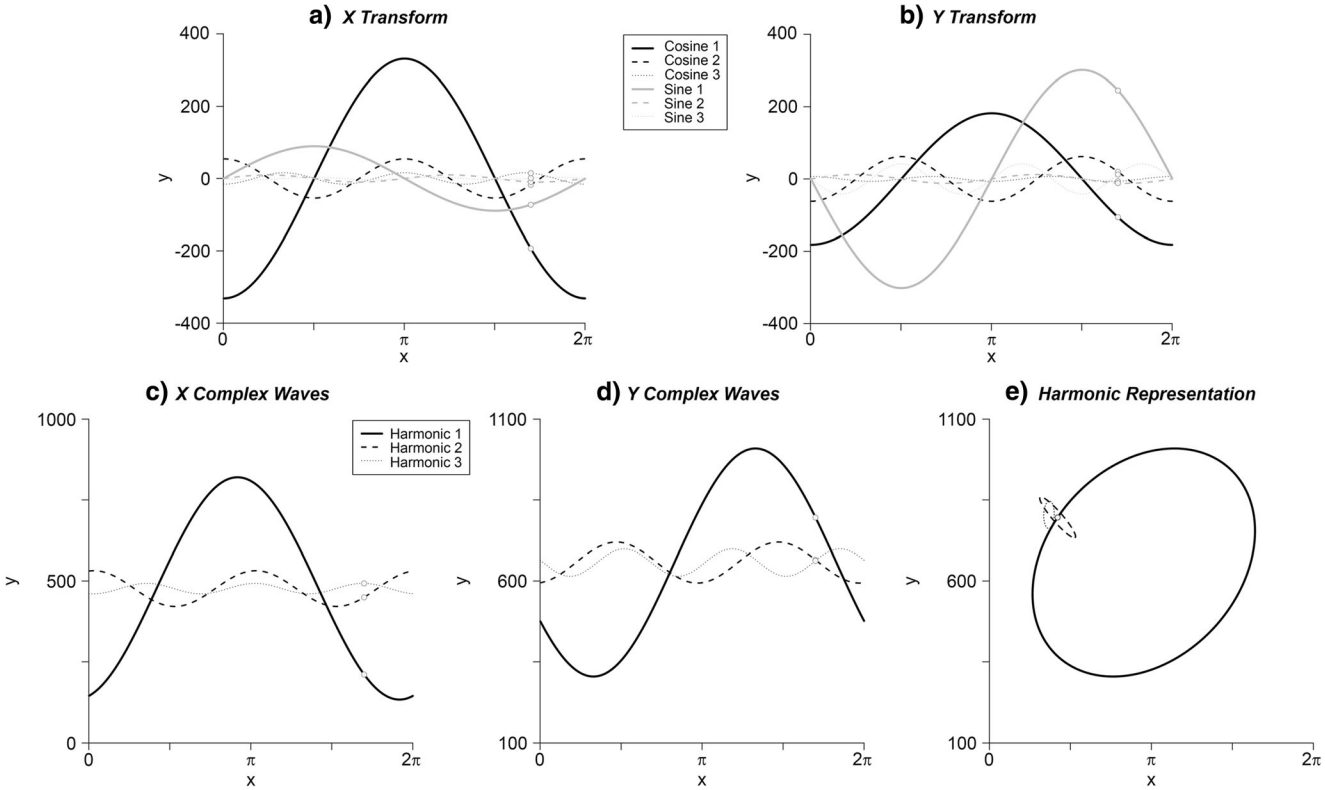

Fig. 6 Plots of the first three harmonics from the skull in Fig. 5. **a** Elliptical Fourier expansion of the *x*-coordinates from Fig. 3 (*X Transform*). **b** Elliptical Fourier expansion of the *y*-coordinates from Fig. 3 (*Y Transform*). **c**, **d** Cosine and sine waves combined to form complex waves for the X and Y transforms (**c** *X* and **d** *Y Complex Waves*). **e** The two complex waves plotted against one another to form an ellipse for each harmonic (reconstructed using the constants (A0, C0) to determine centroid position) (*Harmonic Representation*). Waves for the first harmonic in **c** and **d** are calculated using Eqs. A1 and A2, respectively. *Dot* depicts equivalent point from the skull outline in each plot (point 850 out of 1000). Images created using R [44]

EFA can also be extended to enable 3D shape analysis by adding the following equation for the *z*-axis to Eqs. (2) and (3):

$$z(t) = E_0 + \sum_{n=1}^{k} (E_n \cos nt_n + F_n \sin nt_{n-1}) \quad (6)$$

This results in six Fourier coefficients for each harmonic, two for each axis, instead of the four provided with more traditional 2D EFA.

Coupled with the continuous wavelet transform (CWT), the limitation of the global nature of shape description with EFA can be overcome to provide greater insight into localized shape features [34]. CWT can be beneficial when dealing parts of an outline that contain corners or complex curvatures, as it uses small waves (wavelets), differing in size and starting position, that focus on a specific location [50]. For an in-depth discussion of wavelet theory and application, refer to the theoretical guides provided by Daubechies [42], Lestrel et al. [51], and Neal and Russ [50].

To enable meaningful comparison of multiple objects using EFA, it is necessary that the data be normalized with regards to orientation [6] since elliptical Fourier coefficients rely on a coordinate system. To normalize, Kuhl and Giardina [1] recommend alignment based on the major axis of the first harmonic (Fig. 9). The second optional normalization is for size differences. This can be useful if the aim is to examine shape differences specifically, as considerable size differences (e.g., between sexes) could overpower shape differences. Size correction can be undertaken following Kuhl and Giardina [1], by rescaling the semi-major axis of the first harmonic to a value of one and adjusting all remaining coefficients by the same factor (Fig. 9). Since size is an important factor in sex and ancestry classification [52–55], there are advantages for retaining it in forensic anthropology analyses. For example, Schmittbuhl et al. [17] reported up to a 13% reduction in sex classification accuracies when size was removed from the EFA of the mandible.

An alternative method of size, scale, and translation normalization is Procrustes analysis (GPA). GPA minimizes the sum of the squared differences between a mean and the entire dataset [37]. This is achieved through repetitively choosing an object at random as the mean, before computing a new mean once all samples have been superimposed. GPA has been used for normalization with Fourier methods in studies on artificial cranial deformation [56] and human molar identification [57]. Corny and

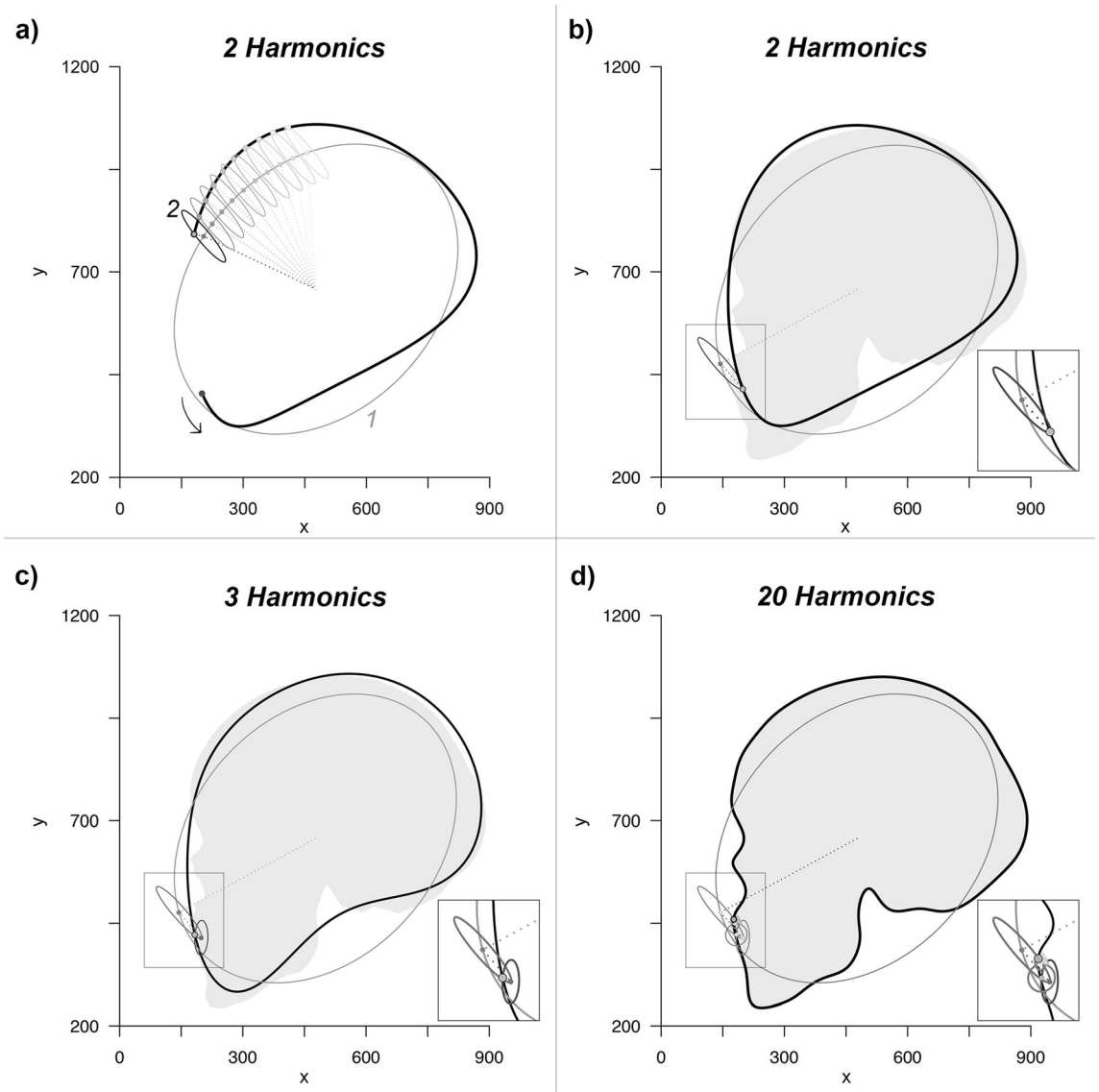

Fig. 7 Inverse representation of elliptical Fourier series depicting **a** the path of traveling around 1000 points on the skull from Fig. 5 using two harmonics, up to point 850, and the shape achieved with all 1000 points using **b** 2, **c** 3, and **d** 20 harmonics. Reconstructed using the constants (A0, C0) to determine centroid position. Harmonics are *gray*; phasors are *dotted lines*, and the combined outlines are *bold black lines*. Images created using R [44]

Detroit [57] specifically compared several normalization procedures on their data, with classification rates calculated using the leave-one-out cross-validation procedure. They concluded that GPA was the most appropriate method for near-circular outlines, with a misclassification rate of 2.8% of isolated molars compared with the traditional Fourier normalization procedure proposed by Kuhl and Giardina [1], which misclassified 3.3% of samples. These marginal differences between normalization approaches may be negligible in many contexts.

A pivotal question is "when to choose EFA as the shape quantifier?" In our view, when the investigator is interested in describing the global shape of a structure as a continuous contour and finds an approximation of the original structure to be sufficient, then EFA may be a suitable choice. In this context, the global nature of the shape description is an advantage and provides the flexibility that the method can be used when homologous landmarks are sparse, difficult to establish, or (less preferably) entirely absent. In some cases, EFA can act as a data reduction technique which may be favorable when it is sufficient to use only a small number of harmonics to approximate the shape. Outside of these contexts, EFA is simply one of several alternatives for shape quantification. In these circumstances, the transformation of spatial data to the frequency domain has been considered to be a superfluous additional step, since the original geometric data can be directly evaluated using other methods [58].

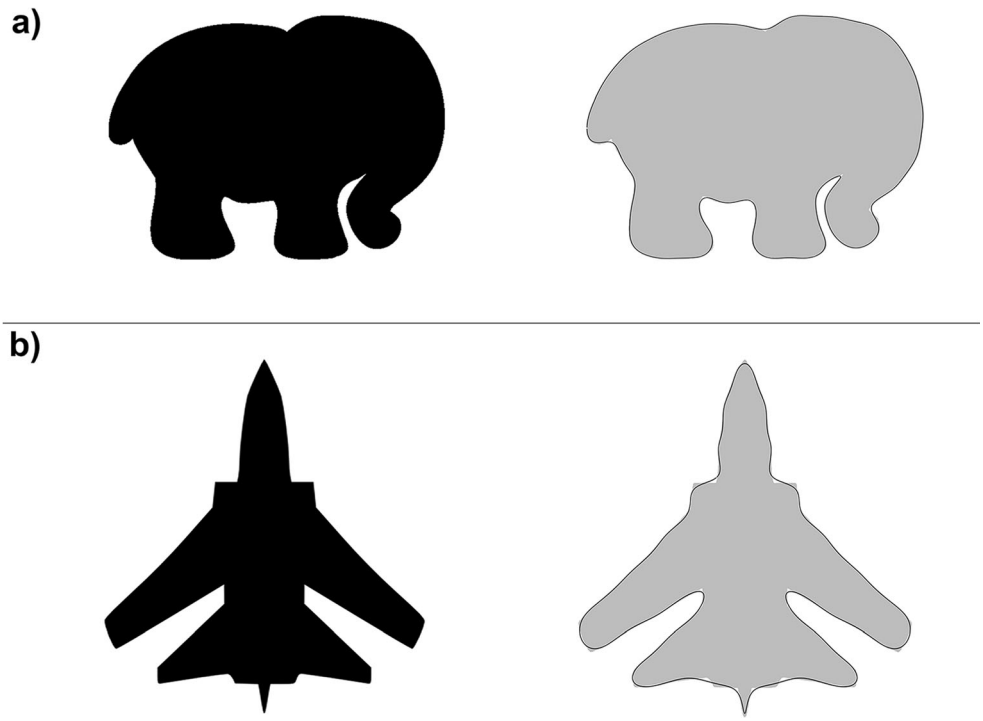

Fig. 8 Elliptical Fourier analysis, using 30 harmonics, of **a** a natural type object (elephant cartoon) and **b** silhouette of a fighter jet. *Left side* shows original image in *black*. *Right side* shows original image (*gray*) with EFA reconstruction (*dark line*). Note the poorer ability of EFA to capture pointed corners and straight edges due to the elliptical nature of the EFA capture process. Starting binarized outlines adapted from clker.com (19/03/15). Elliptical Fourier reconstructions created in R [44]

EFA applications in forensic anthropology

Since its development, there have been a number of studies using EFA to analyze anthropologically relevant topics such as orthodontic treatments [59], age-related changes in mandibular form [60], artificial cranial deformation [56], facial form differences in ancestry [61], sexual dimorphism of the chin [62], as well as one attempt to predict the facial profile from the skull [63]. EFA for forensic identification purposes does not appear until 2000, 18 years after it was described by Kuhl and Giardina [1], with Tanaka and colleagues' study on the proximal humerus [4]. Below, we summarize studies using EFA in a forensic anthropological context based on the skeletal element studied (also see Table 3 for summary).

Skull

The variability of frontal sinus patterns was quantified with EFA and used successfully as an identification tool by Christensen [12, 64]. This was achieved through tracing and digitizing the sinus outlines from radiographs, retaining size information in the elliptical Fourier coefficients. Using log likelihood ratios, Christensen [12] was able to conservatively match frontal sinus images using 20 harmonics, with the odds of a correct match compared with a match from the population reportedly being 10^{21} to 1. Although other researchers have previously quantified frontal sinuses, prior to Christensen, no attempt had been made to measure their individuating power.

Maxwell and Ross [65] explored the utility of cropped cranial vault outlines from radiographs as a differential

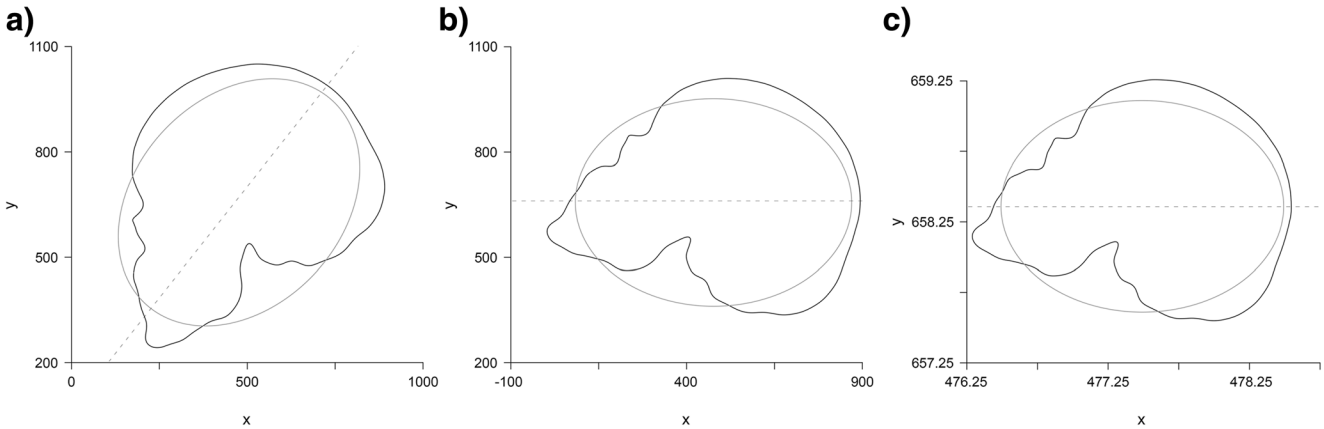

Fig. 9 Elliptical Fourier analysis conducted on a skull image using 40 harmonics. Plots display Fourier reconstructed outline superimposed with the first harmonic (ellipse) using original (**a**), orientation normalized (**b**), and size and orientation normalized (**c**) EFA methods. *Dotted line* represents major axis of the first harmonic, which is aligned to the *x*-axis using the orientation normalized method. Images created using R [44]

Table 3 Summary of skeletal studies utilizing elliptical Fourier analysis in a forensic anthropology context

Skeletal element		Study	Purpose
Cranial	Frontal sinus	Christensen [12, 64]	Identification
	Cranial vault	Maxwell and Ross [65]	Identification
	Craniofacial complex	Lestrel et al. [51]	Sex estimation
	Orbits	Gore et al. [44]	Sex, age, ancestry estimation
	Anterior nasal aperture	McDowell et al. [15]	Ancestry estimation
Infracranial	Mandible	Schmittbuhl et al. [17]	Sex estimation
	Clavicle	Stephan et al. [22, 68]	Identification
	Vertebrae	Paolello and Cabo-Perez [70]	Identification
	Proximal humerus	Tanaka et al. [4]	Sex estimation
	Greater sciatic notch	Velemínská et al. [25]	Sex estimation
	Patella	Niespodziewanski et al. [31]	Identification

identifying feature. Outlines were manually traced from nasion to the mastoid processes, with 30 harmonics used for analysis, normalizing for size. While they recommend EFA as an analytical tool, they found much less value for EFA of the outline shape as an identification tool, concluding that the shape of the vault outline alone is not varied enough to individuate. Their conclusion was supported by a supplementary visual comparison test, in which only 47% of assessors correctly assigned all radiographs [65]. It may be worth noting that despite the authors own recommendation for using EFA with a multivariate analysis of variance (MANOVA) or discriminant function analysis (DFA), this study used univariate *t* tests for analysis.

Using EFA, Lestrel et al. [54] describes, in detail, the sexual dimorphism of the craniofacial complex. Their study aimed to highlight shape variations specifically, and therefore, the study was conducted on size-normalized Fourier coefficients. Sourcing data from multiple studies, statistically significant sexually dimorphic changes were evident in all structures examined, namely the nasal bones, cranial base, dental arch, mandibular arch, and cranial vault. The most sexually dimorphic region was that of the nasal bones, which were longer and narrower in females, while the slightest dimorphism was noted for the cranial vault [54].

Gore et al. [48] used EFA to assess the influence of sex, age, ancestry, and geographical location on size-normalized orbital shape. Photographs were taken of 162 individuals sourced from skeletal collections in the USA and South Africa. They demonstrated that orbital outlines could effectively distinguish individuals based on sex, ancestry, and geographical location. While they speculated that age may affect orbital size in relation to the rest of the craniofacial complex, Gore et al. [48] did not observe any age-related influence on its shape as an isolated structure.

In 2012, McDowell et al. [15] analyzed the shape of the anterior nasal aperture in South Africans with EFA to quantify population differences. Traditional landmark craniometrics and GPA were also used. The EFA analysis was conducted on photographs with digitally traced outlines. Size-normalized EFA enabled classification with 94% accuracy for ancestry estimation, which is comparable to their reported 94–95% accuracy using craniometrics [15]. This is an improvement on the 83–86% accuracy rates reported for visual assessment [16].

In 2002, Schmittbuhl et al. [17] studied individual variability and sexual dimorphism in mandibular shape using EFA. Instead of conducting analysis on the customary Fourier coefficients, they defined novel "elliptical descriptors," based on axis length, axis orientation, and initial phase angle. These descriptors were designed to enable ease of association to morphological interpretation [17]. They were able to successfully classify 97% of males and 92% of females from the shape and size of the lateral mandible outline. With the removal of the size factor, they achieved classification rates of 84 and 81% in males and females, respectively. The size-retained data thereby provide a marked improvement on classification accuracies using both visual assessment (58–86% [21]) and linear measurements (78–85% [18–20]).

The EFA-CWT method previously described has been utilized in anthropological studies on sexual dimorphism in the human cranial base [34, 51] and cranial vault [66]. However, it has not been applied in a forensic setting thus far. The 3D EFA approach has been employed with skeletal material in a forensic context, with a study assessing the influence of ancestral group, sex, and age on orbital margins [67].

Clavicle

Post-mortem clavicle outlines were recently compared with ante-mortem records to aid in skeletal identification by Stephan et al. [22, 68, 69]. Using the sum of squared differences in normalized Fourier descriptors between 3D clavicle laser scans and clavicle morphologies recorded on ante-mortem chest radiographs, true positive matches were found in the top 5% of the shape-ranked chest radiograph

databases 75% of the time [22, 68]. These results offer major benefits for automated searching of large datasets in contrast to manual searches.

Vertebrae

Paolello and Cabo-Perez [70] employed EFA to assess individuation of vertebral outlines from radiographs. The outlines of the left transverse process of 85-s lumbar vertebra were extracted from radiographs that were conducted to simulate ante-mortem and post-mortem records. While correction for size was not specified in the written account, nor were the classification accuracies, these authors recommended use of the method for forensic casework [70].

Humerus

In 2000, Tanaka et al. utilized EFA to quantify sexual dimorphism of the proximal humerus in Japanese adults born *c.*1900 [4]. The humeral outlines from photographs were traced and digitized, before conducting EFA using 27 harmonics. Data were analyzed using a one-way MANOVA, with Wilk's lambda scores showing statistically significant sex differences. While significant sex differences in size were noted, they still achieved a correct classification of sex in approximately 92–95% of humeri using discriminant functions based on size-normalized amplitudes. Reconstruction of the Fourier coefficients revealed male humeri to possess a more pronounced lesser tubercle but a less pronounced greater tubercle [4]. Outline analysis performed better in terms of accuracy than both linear measurement (89–90% [24]) and visual assessment (83–86% [18]) methods.

Os coxae

Velemínská et al. [25] conducted a study in 2013 on sexual dimorphism of the greater sciatic notch using the following six geometric morphometric techniques: (1) with equally angled semi-landmarks from a center point, (2) distances between those landmarks and the center point, (3) semi-landmarks equidistant to the curve, (4) polyline distances, (5) Fourier coefficients, and (6) Legendre coefficients. All methods were conducted after size normalization and proved to successfully classify sex (90–92%), with the Fourier coefficients classifying with the highest accuracy. EFA also outperformed visual assessment studies, which classified sex with 80–88% accuracy [28–30]. Classification accuracy declined as the number of harmonics increased above the optimum number (in this case, five), most likely due to a reduction of the signal to noise ratio.

Patella

Niespodziewanski et al. [31] recently assessed the utility of lateral patella outlines for individuation using EFA. In a similar fashion to Stephan et al. [22, 68], patella outlines were compared between radiographs and rotated shadowgrams from 3D laser scans. Based on ranking the sum of squared differences between the elliptical Fourier coefficients, 20 of the 22 specimens ranked in the top five images (top 1.4%), with 16 of the 22 correctly matching the top ranked image.

EFA software

The calculations involved in EFA are laborious by hand, especially when large numbers of harmonics are used, which lends the methods entirely to computerized approaches. Since EFA's first conception in 1982, several programs have been developed to specifically undertake EFA. The majority of these are available online for free download.

Christensen's frontal sinus research [12, 64] employed *EFAWin* (now called *EFAV* on the SUNY Stony Brook website) developed by Mike Isaev [71] for conducting elliptical Fourier analysis and obtaining the Fourier coefficients. The Fourier calculations for the software were done by Rohlf and Ferson, who also released their own software a couple years earlier [72] that can be used in conjunction with their outline coordinate extraction software tpsDig [73].

SHAPE was developed in 2002 by Iwata and Ukai [74] and is a software package that includes five programs to perform image outline extraction, run normalized EFA and principal component analysis, as well as visualize outline reconstructions at each stage. The image outline is extracted using edge detection on an optimized image: Each image is separated into three based on the RGB channels, and the image with the highest object-to-background contrast is selected to undergo automatic threshold establishment for binarization [74]. This program has been used by Stephan et al. [22] in initial trials of clavicle matching and by Maxwell and Ross in their study on identification from cranial vault outlines [65].

Momocs [75] is an EFA package recently developed for use within the R environment [44]. The functions written within *Momocs* are primarily derived from Claude's 2008 book *Morphometrics Using R* [49]. It encompasses the majority of the analytical process, including outline extraction, EFA, as well as statistical methods such as principal component analysis, MANOVA, and thin plate splines. The utility of calling individual functions within R allows the user to customize the analysis to their needs; however, it also requires a basic knowledge of R programming to navigate. Despite its use in a wide range of other research areas (e.g., sexual dimorphism of bird tails [76], phenotypic gene expression patterns [77], and a comparison of Middle Stone Age assemblages [78]),

Momocs has not been used in the forensic anthropological literature so far.

To conduct their chest radiograph comparison studies, Stephan et al. [22] coded EFA equations from Kuhl and Giardina [1] into R as part of their customized clavicle matching software. Rather than enabling generalized use of EFA, this software instead provides a dedicated standalone tool for ranking radiographs based on EFA encoding. While originally designed for clavicles, the program has also been successfully extended to searching of lateral knee radiographs from 3D scans of patellae [31].

PAleontological STatistics (*PAST*) [79] was developed as a comprehensive tool for paleontological data analysis, permitting EFA on already obtained outline coordinates. This software has not yet made an appearance using EFA in the forensic anthropological literature.

There are also some commercially available software packages for EFA. The *EFF23* software is one of the longest available, developed around 30 years ago as a MS-DOS tool for running EFA on a matrix of coordinates [7, 80]. The elliptical Fourier coefficients are then exported to analyze in third-party statistical software. This software has been used in combination with *MLmetrics* to digitize outlines, also available from the *EFF23* developers [6, 80], and has been used by Tanaka et al. [4] in their proximal humerus study. Another shape analysis program that includes EFA among a number of shape routines is *NTSYSpc* developed by Rohlf [81]. This program also requires a third-party outline digitization tool to be used ahead of the EFA.

The above options provide investigators with a range of solutions. While user preferences are likely to vary, programs with graphical user interfaces (GUIs) may generally be more convenient for investigators without coding experience. The trade-off is that these programs offer much less flexibility compared to those running from coding consoles. Out of the GUI programs available, SHAPE offers a simple, easy to install, and user-friendly workflow that includes the outline extraction in one program suite that some researchers may find advantageous.

The future

Modern day computers offer abundant power to undertake EFA, that only require seconds for analysis. Consequently, the scope to increase the use of EFA in forensic anthropology within the computer age is immense, in part because bones are natural objects with smooth curving outlines. Future applications may include, for example, sex and ancestry estimation of skulls and osteometric sorting based on longitudinal or cross-sectional bone shape and may extend beyond forensic anthropology to other disciplines of legal medicine—a ready example is forensic odontology given that EFA has already been used for growth studies of teeth [82]. The possibilities are massive, as recently demonstrated by the automated searching of radiographic libraries for identification purposes.

One of the major attractions to EFA is that it can be undertaken using a broad array of acquisition equipment from relatively simple digital cameras (e.g., Tanaka et al. [4]) to more complex 3D scanning units (e.g., 3D digitizer used by Urbanová [67]). All these factors award EFA special utility where large samples are concerned and yield potential for a Fordisc-like anthropometric tool based on EFA to be developed.

References

1. Kuhl F, Giardina C (1982) Elliptic Fourier features of a closed contour. Comput Graphics Image Process 18:236–258. doi:10.1016/0146-664X(82)90034-X
2. Herivel J (1975) Joseph Fourier: the man and the physicist. Oxford University Press, Oxford
3. Cosgriff RL (1966) Identification of shape. Report No. 820–11 of the Ohio State University Research Foundation. ASTIA Identification AD 254 792
4. Tanaka H, Lestrel P, Uetake T, Susumu K, Ohtsuki F (2000) Sex differences in proximal humeral outline shape: elliptical Fourier functions. J Forensic Sci 45(2):292–302. doi:10.1520/JFS14682J
5. Crampton J (1995) Elliptic Fourier shape analysis of fossil bivalves: some practical considerations. Lethaia 28(2):179–186. doi:10.1111/j.1502-3931.1995.tb01611.x
6. Lestrel P (1989) Method for analyzing complex two-dimensional forms: elliptical Fourier functions. Am J Human Biol 1:149–164. doi:10.1002/ajhb.1310010204
7. Lestrel P (1997) Fourier descriptors and their applications in biology. Cambridge University Press, Cambridge; New York
8. Lestrel P (1997) Morphometrics of craniofacial form. In: Dixon D, Hoyte DAN, Ronning O (eds) Fundamentals of craniofacial growth. CRC Press, Boca Raton, FL, pp 155–187
9. Nixon M, Aguado A (2008) Feature extraction and image processing, 2nd edn. Elsevier Academic Press, Oxford
10. Swiderski DL, Zelditch ML, Fink WL (2002) Comparability, morphometrics and phylogenetic systematics. In: MacLeod N, Forey PL (eds) Morphology, shape and phylogeny. Systematics Association Special Volumes. CRC Press, Boca Raton, FL, pp 67–99
11. Transnational College of Lex (2012) Who is Fourier? A mathematical adventure (trans: Gleason a), 2nd edn. Language Research Foundation, Cambridge, MA
12. Christensen AM (2005) Testing the reliability of frontal sinuses in positive identification. J Forensic Sci 50(1):18–22. doi:10.1520/JFS2004145
13. Kullman L, Eklund B, Grundin R (1990) The value of the frontal sinus in identification of unknown persons. J Forensic Odontostomatol 8(1):3–10
14. Cryer M (1907) Some variations in the frontal sinuses. JAMA 48 (4):284–289. doi:10.1001/jama.1907.25220300012001d
15. McDowell J, L'Abbé E, Kenyhercz M (2012) Nasal aperture shape evaluation between black and white South Africans. Forensic Sci Int 222(1–3):397 . doi:10.1016/j.forsciint.2012.06.007e391-396
16. Hefner J (2014) Cranial morphoscopic traits and the assessment of American black, American white, and Hispanic ancestry. In: Berg GE, Ta'ala SC (eds) Biological affinity in forensic identification of human skeletal remains: beyond black and white. Taylor & Francis Group, Boca Raton, FL, pp 27–42

17. Schmittbuhl M, Le Minor J, Schaaf A, Mangin P (2002) The human mandible in lateral view: elliptical Fourier descriptors of the outline and their morphological analysis. Ann Anat 184(2):199–207. doi:10.1016/S0940-9602(02)80021-8
18. Spradley K, Jantz R (2011) Sex estimation in forensic anthropology: skull versus postcranial elements. J Forensic Sci 56(2):289–296. doi:10.1111/j.1556-4029.2010.01635.x
19. Steyn M, İşcan MY (1998) Sexual dimorphism in the crania and mandibles of south African whites. Forensic Sci Int 98(1–2):9–16. doi:10.1016/S0379-0738(98)00120-0
20. Giles E (1964) Sex determination by discriminant function analysis of the mandible. Am J Phys Anthropol 22(2):129–135. doi:10.1002/ajpa.1330220212
21. Williams B, Rogers T (2006) Evaluating the accuracy and precision of cranial morphological traits for sex determination. J Forensic Sci 51(4):729–735. doi:10.1111/j.1556-4029.2006.00177.x
22. Stephan C, Emanovsky P, Tyrrell A (2009) The use of clavicle boundary outlines to identify skeletal remains of US personnel recovered from past conflicts: results of initial tests. Paper presented at the Biological Shape Analysis: proceedings of the 1st international symposium, Tsukuba, Japan, 3–6 June 2009
23. Stephan C, Winburn A, Christensen A, Tyrrell A (2011) Skeletal identification by radiographic comparison: blind tests of a morphoscopic method using antemortem chest radiographs. J Forensic Sci 56(2):320–332. doi:10.1111/j.1556-4029.2010.01673.x
24. Dittrick J, Suchey J (1986) Sex determination of prehistoric central California skeletal remains using discriminant analysis of the femur and humerus. Am J Phys Anthropol 70:3–9. doi:10.1002/ajpa.1330700103
25. Velemínská J, Krajíček V, Dupej J, Goméz-Valdés J (2013) Technical note: geometric morphometrics and sexual dimorphism of the greater sciatic notch in adults from two skeletal collections: the accuracy and reliability of sex classification. Am J Phys Anthropol 152(4):558–565. doi:10.1002/ajpa.22373
26. Steyn M, İşcan MY (2008) Metric sex determination from the pelvis in modern Greeks. Forensic Sci Int 179(1):86.e81–86.e86. doi:10.1016/j.forsciint.2008.04.022
27. Patriquin ML, Steyn M, Loth SR (2005) Metric analysis of sex differences in south African black and white pelves. Forensic Sci Int 147(2–3):119–127. doi:10.1016/j.forsciint.2004.09.074
28. Walker P (2005) Greater sciatic notch morphology: sex, age, and population differences. Am J Phys Anthropol 127(4):385–391. doi:10.1002/ajpa.10422
29. Rogers T, Saunders S (1994) Accuracy of sex determination using morphological traits of the human pelvis. J Forensic Sci 39(4):1047–1056. doi:10.1016/1353-1131(95)90091-8
30. Patriquin ML, Loth SR, Steyn M (2003) Sexually dimorphic pelvic morphology in south African whites and blacks. Homo 53(3):255–262. doi:10.1078/0018-442X-00049
31. Niespodziewanski E, Stephan CN, Guyomarc'h P, Fenton TW (2016) Human identification via lateral patella radiographs: a validation study. J Forensic Sci 61(1):134–140. doi:10.1111/1556-4029.12898
32. Trotter M, Gleser G (1952) Estimation of stature from long bones of American whites and negroes. Am J Phys Anthropol 10(4):463–514. doi:10.1002/ajpa.1330100407
33. National Research Council (2009) Strengthening forensic science in the United States: a path forward. National Academies Press, Washington, D.C
34. Lestrel P, Cesar R Jr, Takahashi O, Kanazawa E (2004) A Fourier-wavelet representation of 2-D shapes: sexual dimorphism in the Japanese cranial base. Anthropol Sci 112(1):3–28. doi:10.1537/ase.00069
35. Martin R (1928) Lehrbuch der anthropologie in systematischer darstellung: mit besonderer berücksichtigung der anthropologischen methoden für studierende ärtze und forschungsreisende. Gustav Fischer, Jena
36. Jantz R, Ousley S (2005) FORDISC 3.1: personal computer forensic discriminant functions. The University of Tennessee, Knoxville
37. Gower J (1975) Generalized Procrustes analysis. Psychometrika 40(1):33–51. doi:10.1007/BF02291478
38. Rohlf F, Slice D (1990) Extensions of the Procrustes method for the optimal superimposition of landmarks. Systematic Zool 39(1):40–59. doi:10.2307/2992207
39. Bookstein FL (1991) Morphometric tools for landmark data: geometry and biology. Cambridge University Press, Cambridge
40. Lele S (1991) Some comments on coordinate-free and scale-invariant methods in morphometrics. Am J Phys Anthropol 85(4):407–417. doi:10.1002/ajpa.1330850405
41. Bookstein F (1997) Landmark methods for forms without landmarks: morphometrics of group differences in outline shape. Med Image Anal 1(3):225–243. doi:10.1016/S1361-8415(97)85012-8
42. Daubechies I (1992) Ten lectures on wavelets, vol 61. Society for Industrial and Applied Mathematics, Philadelphia, PA
43. Rohlf F (1986) Relationships among eigenshape analysis, Fourier analysis, and analysis of coordinates. Math Geol 18(8):845–854. doi:10.1007/BF00899747
44. R Core Team (2013) R: a language and environment for statistical computing. R Foundation for Statistical Computing. http://www.R-project.org.
45. Rohlf F, Archie J (1984) A comparison of Fourier methods for the description of wing shape in mosquitoes (Diptera: Culicidae). Systematic Zool 33(3):302–317. doi:10.2307/2413076
46. Zahn C, Roskies R (1972) Fourier descriptors for plane closed curves. IEEE Trans Comput C-21(3):269–281
47. Zhang DS, Lu G (2002) A comparative study of Fourier descriptors for shape representation and retrieval. In: Proceedings of the Fifth Asian Conference on Computer Vision (ACCV02), Melbourne, Australia, January 22–25. pp 646–651
48. Gore T, Nawrocki S, Langdon J, Bouzar N The use of elliptical Fourier analysis on orbit shape in human skeletal remains. Paper presented at the Biological Shape Analysis: proceedings of the 1st international symposium, Tsukuba, Japan, 3–6 June, 2009
49. Claude J (2008) Morphometrics with R. Springer-Verlag, New York, NY
50. Neal F, Russ J (2012) Measuring shape. CRC Press, Boca Raton, FL
51. Lestrel P, Cesar R, Takahashi O, Kanazawa E (2005) Sexual dimorphism in the Japanese cranial base: a Fourier-wavelet representation. Am J Phys Anthropol 128(3):608–622. doi:10.1002/ajpa.20209
52. Howells WW (1973) Cranial variation in man: a study by multivariate analysis of patterns of difference among recent human populations. Harvard University Press, Cambridge
53. Ferrario V, Sforza C, Schmitz J, Miani A, Taroni G (1995) Fourier analysis of human soft tissue facial shape: sex differences in normal adults. J Anat 187(3):593–602
54. Lestrel P, Kanazawa E, Wolfe C (2011) Sexual dimorphism using elliptical Fourier analysis: shape differences in the craniofacial complex. Anthropol Sci 119(3):213–229. doi:10.1537/ase.100630
55. Stewart T (1979) Essentials of forensic anthropology, especially as developed in the United States. Charles C, Thomas, Springfield, IL
56. Frieß M, Baylac M (2003) Exploring artificial cranial deformation using elliptical Fourier analysis of Procrustes aligned outlines. Am J Phys Anthropol 122(1):11–22
57. Corny J, Detroit F (2014) Technical note: anatomic identification of isolated modern human molars: testing Procrustes aligned outlines as a standardization procedure for elliptic Fourier analysis. Am J Phys Anthropol 153(2):314–322. doi:10.1002/ajpa.22428
58. MacLeod N (2012) The center cannot hold II: elliptical Fourier analysis. PalaeoMath 101(79):29–42

59. Lestrel P, Kerr W (1993) Quantification of function regulator therapy using elliptical Fourier functions. Eur J Orthod 15(6):481–491. doi:10.1093/ejo/15.6.481
60. Chen S, Lestrel P, Kerr W, McColl J (2000) Describing shape changes in the human mandible using elliptical Fourier functions. Eur J Orthod 22:205–216. doi:10.1093/ejo/22.3.205
61. Sheridan C, Thomas C, Clement J (1997) Quantification of ethnic differences in facial profile. Aust Orthod J 14(4):218–224
62. Thayer ZM, Dobson SD (2010) Sexual dimorphism in chin shape: implications for adaptive hypotheses. Am J Phys Anthropol 143(3): 417–425. doi:10.1002/ajpa.21330
63. Rose A, Woods M, Clement J, Thomas C (2003) Lateral facial soft-tissue prediction model: analysis using Fourier shape descriptors and traditional cephalometric methods. Am J Phys Anthropol 121 (2):172–180. doi:10.1002/ajpa.10173
64. Christensen A (2004) Assessing the variation in individual frontal sinus outlines. Am J Phys Anthropol 127(3):291–295. doi:10.1002/ajpa.20116
65. Maxwell A, Ross A (2014) A radiographic study on the utility of cranial vault outlines for positive identifications. J Forensic Sci 59 (2):314–318. doi:10.1111/1556-4029.12346
66. Lestrel P, Cesar Jr R, Wolfe C, Ohtsuki F Computational shape analysis: based on a Fourier-wavelet representation of the fossil human cranial vault. Paper presented at the Biological Shape Analysis: proceedings of the 1st international symposium, Tsukuba, Japan, 3–6 June, 2009
67. Urbanová P Variation of the orbital rim using elliptical fourier analysis. Paper presented at the Biological Shape Analysis: proceedings of the 1st international symposium, Tsukuba, Japan, 3–6 June, 2009
68. Stephan C, Amidan B, Trease H, Guyomarc'h P, Pulsipher T, Byrd J (2014) Morphometric comparison of clavicle outlines from 3D bone scans and 2D chest radiographs: a shortlisting tool to assist radiographic identification of human skeletons. J Forensic Sci 59(2):306–313. doi:10.1111/1556-4029.12324
69. D'Alonzo S, Guyomarc'h P, Byrd J, Stephan CN (2017) A large-sample test of a semi-automated clavicle search engine to assist skeletal identification by radiograph comparison. J Forensic Sci In Press
70. Paolello J, Cabo-Perez L (2008) Elliptical Fourier analysis of vertebral outlines for victim identification. In: AAFS (ed) Proceedings of the American Academy of Forensic Sciences 60th annual scientific meeting, Washington, DC, 2008. p 367
71. Isaev M (1995) EFAV. Morphometrics at SUNY Stony Brook, http://life.bio.sunysb.edu/morph/
72. Rohlf F (1993) EFA. Morphometrics at SUNY Stony Brook, http://life.bio.sunysb.edu/morph/
73. Rohlf F (1997) tpsDig. Morphometrics at SUNY Stony Brook, http://life.bio.sunysb.edu/morph/
74. Iwata H, Ukai Y (2002) SHAPE: a computer program package for quantitative evaluation of biological shapes based on elliptic Fourier descriptors. J Hered 93(5):384–385. doi:10.1093/jhered/93.5.384
75. Bonhomme V, Picq S, Gaucherel C, Claude J (2014) Momocs: outline analysis using R. J Stat Softw 56(13):1–24
76. Felice RN, O'Connor PM (2016) The evolution of sexually dimorphic tail feathers is not associated with tail skeleton dimorphism. J Avian Biol 47(3):371–377. doi:10.1111/jav.00801
77. Martínez-Abadías N, Mateu R, Niksic M, Russo L, Sharpe J (2015) Geometric morphometrics on gene expression patterns within phenotypes: a case example on limb development. Syst Biol 65(6): 194–211. doi:10.1093/sysbio/syv067
78. Archer W, Pop CM, Gunz P, McPherron SP (2016) What is still bay? Human biogeography and bifacial point variability. J Hum Evol 97:58–72. doi:10.1016/j.jhevol.2016.05.007
79. Hammer Ø (2001) PAST: paleontological statistics software package for education and data analysis. Palaeontol Electronica 4(1):9pp
80. Wolfe C, Lestrel P, Read D (1998) EFF23 2-D and 3-D elliptical Fourier functions. Software Description and User's Manual v3.0, CA
81. Rohlf F (2008) NTSYSpc: numerical taxonomy system, ver. 2.20. Exeter Publishing, Ltd, Setauket, NY
82. Richards LC, Townsend GC, Kasai K (1997) Application of the Fourier method on genetic studies of dentofacial morphology. In: Lestrel PE (ed) Fourier descriptors and their applications in biology. Cambridge University Press, Cambridge, pp 189–209. doi:10.1017/CBO9780511529870.009